Plasmon bands in multilayer graphene

P. Wachsmuth,[1,*] R. Hambach,[1] G. Benner,[2] and U. Kaiser[1]

[1]*Electron Microscopy Group of Materials Science, Ulm University, Albert-Einstein-Allee 11, 89081 Ulm, Germany*

[2]*Carl Zeiss Microscopy GmbH, Carl-Zeiss-Straße 22, 73447 Oberkochen, Germany*

(Received 13 June 2014; revised manuscript received 17 November 2014; published 29 December 2014)

High-energy collective electronic excitations (plasmons) in freestanding multilayer graphene are studied by momentum-resolved electron energy-loss spectroscopy (EELS). For normal incidence, only the high-energy plasmon band is excited and we measure a blueshift of the π-plasmon dispersion with increasing thickness. The observed transition between two-dimensional and three-dimensional behavior is explained using a layered-electron-gas (LEG) model. We propose a method to measure all individual plasmon bands by tilting the sample with respect to the electron beam. As a proof of concept, EELS experiments for three-layer graphene are compared with predictions from the LEG model.

DOI: 10.1103/PhysRevB.90.235434 PACS number(s): 79.20.Uv, 81.05.ue, 73.21.Ac, 71.45.Gm

I. INTRODUCTION

Collective electronic excitations (plasmons) in single- and multilayer graphene have attracted a great deal of attention because of their importance for plasmonic and optoelectronic devices [1,2]. This interest is largely motivated by the high tunability of charge-carrier plasmons and the optical absorption of graphene [2], which allow applications in many devices, such as photodetectors [3] or ultrafast lasers [4]. Graphene can also be combined with other two-dimensional (2D) crystals, e.g., insulating hexagonal boron nitrite (hBN) or semiconducting molybdenum disulfide (MoS_2) to create a multitude of artificial heterostructures. The electronic properties of such novel multilayer structures can be tailored for an even larger range of possible applications as well as for the study of novel physical phenomena [5,6].

Plasmons in these 2D-based multilayers can be understood as charge oscillations confined to certain planes and coupled via interlayer Coulomb interactions. If the coupling is weak, plasmon excitations on each of the N layers behave like in an isolated sheet. But a strong interlayer coupling lifts the degeneracy of these plasmon modes and leads to the formation of N plasmon bands. In the past, plasmon bands have been investigated extensively in macroscopic multilayers, such as metallic superlattices and semiconductor quantum-well structures, by a variety of theoretical methods [7–12]. While most experimental studies were performed using (angle-resolved) Raman spectroscopy [13–15], also a few reports from electron energy-loss spectroscopy (EELS) exist [16,17]. The question arises, whether these results remain valid for atomically thin layers. So far, plasmon bands in 2D-based multilayers have only been studied theoretically [18,19], but a detailed experimental verification is still missing. For this purpose, multilayer graphene is an ideal test system as the interlayer distance is well defined and the number of layers of a sample can be controlled with the highest accuracy. In contrast to experiments on epitaxial graphene [20–22], where mainly low-energy charge-carrier plasmons (<3 eV) have been considered, we will focus on the high-energy plasmon bands (>5 eV) in *freestanding* samples. The plasmon-band dispersion is therefore not affected by the screening of a substrate or different doping on the individual sheets. High-energy plasmons in freestanding single- and multilayer graphene were first investigated in the limit of small momentum transfers ($q \to 0$): experimentally by scanning transmission electron microscopy (STEM) EELS [23] and theoretically by *ab initio* simulations [24–27]. The full momentum dependence ($q > 0$) was studied by a variety of theoretical methods [18,28–32] and has been measured recently for single-layer graphene using momentum-resolved EELS [33,34].

In this paper, we present an experimental proof of the formation of plasmon bands in multilayer graphene. To this end, we have measured the π-plasmon dispersion in freestanding multilayer graphene with two to six layers using momentum-resolved EELS in a transmission electron microscope. We use a layered-electron-gas model to explain the observed plasmon dispersion and to discuss the transition from 2D to 3D behavior. In contrast to previous studies [18,19], we combine this simple model with *ab initio* calculations for single-layer graphene, which provides a quantitative and parameter-free prediction of plasmon bands in multilayers. Finally, we propose a method to measure the dispersion of all individual plasmon bands by choosing particular scattering geometries, where only a single plasmon mode is excited. This method is exemplified by momentum-resolved EELS experiments on three-layer graphene.

II. METHODS

The momentum dependence (dispersion) of the plasmon energies in freestanding multilayer graphene has been investigated by electron energy-loss spectroscopy in a transmission electron microscope (TEM). Samples for TEM and EELS investigations were prepared by transferring mechanically exfoliated, thin graphite flakes onto holey carbon grids [35]. The thickness of the prepared flakes was determined by high-resolution TEM imaging performed on a TITAN 80-300 operated at 80 kV. Momentum-resolved energy-loss spectra were recorded at 40 kV on the SALVE I (Sub-Angstrom Low-Voltage Electron Microscopy) prototype [36]. A small, homogeneous part of the sample of about 80 nm diameter has been selected for each EELS experiment using a selected-area aperture. In contrast to standard EELS, we recorded

*philipp.wachsmuth@uni-ulm.de

spectra for a large range of different momentum transfers $\boldsymbol{q}$ simultaneously in the form of ω-q maps (for details see Refs. [34,37] and Supplemental Material [38]). As long as the sample is oriented perpendicular to the electron beam, the probed momentum transfers $\boldsymbol{q}$ are nearly parallel to the graphene sheets and thus coincide with the in-plane component $\bar{\boldsymbol{q}} \approx \boldsymbol{q}$. A momentum resolution of 0.2 Å^{-1} and an energy resolution of 0.3 eV was achieved.

III. RESULTS AND DISCUSSION

A. Plasmon dispersion in multilayer graphene

Figure 1(a) shows a set of experimental energy-loss spectra of multilayer graphene with two to six layers for a fixed in-plane momentum transfer $\bar{q} \approx 0.3\,\text{Å}^{-1}$ along ΓM. Like in graphene and graphite, the spectra feature two characteristic high-energy plasmon peaks, i.e., the π plasmon below 10 eV and the $\pi + \sigma$ plasmon above 15 eV [24,39,40]. We have carefully assessed experimental errors that can alter the line shape, width, and energy of the observed plasmon peaks: (i) Due to the finite momentum resolution, a weighted superposition of spectra with different momentum transfers $\bar{\boldsymbol{q}}$ is measured. As we have shown earlier [34], this leads to a broadening and blueshift of the observed plasmon peaks for very small $\bar{q}$ up to 0.1 Å^{-1}, while spectra at higher $\bar{q}$ remain unaffected. (ii) Contamination on the graphene samples can mask the intrinsic dielectric response. However, the π-plasmon position in single-layer graphene remains rather insensitive to contamination-related effects which in addition become less important as the thickness increases [37].

Starting from the experimental energy-loss spectra, the energy of the π plasmon was determined manually for different $\bar{q}$. The resulting plasmon dispersion curves are shown in Fig. 1(b) for different multilayer systems, as well as for single-layer graphene (dashed black lines, from Ref. [34]) and graphite (solid black lines). The dispersion for graphite was extracted

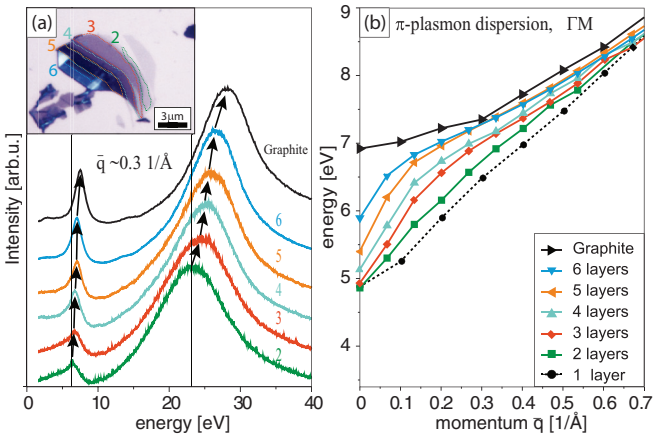

FIG. 1. (Color online) Momentum-resolved electron energy-loss experiments for different positions on a freestanding, multilayer graphene flake (see inset). (a) EEL spectra for a fixed in-plane momentum transfer $\bar{q} \approx 0.3$ Å^{-1} along the ΓM direction. (b) Measured dispersion of the π plasmon for two to six graphene layers. For comparison, also the plasmon dispersion for graphite and single-layer graphene [34] is indicated.

from spectra recorded on a separate sample under comparable conditions. In all cases, peak positions were determined with an estimated reading error of about 0.2 eV. In the limit of $\bar{q} \to 0$, we observe a gradual blueshift of the π plasmon from 4.9 eV (single layer) to around 5.9 eV (six layers), which is still about 1 eV below the peak position found in bulk graphite. This is in good agreement with earlier studies, which where performed using STEM-EELS and are thus restricted to small $\bar{q}$ [24,41]. For very large $\bar{q}$, the dispersion curves for different multilayers converge: at 0.7Å^{-1} the π plasmon in graphene is found only about 0.5 eV below its counterpart in bulk graphite, while for six layers the π-plasmon positions coincide. This trend can be understood intuitively, considering that the electrostatic potential of a plane-wave charge oscillation with wavelength $\lambda = 2\pi/\bar{q}$ in a two-dimensional electron gas drops exponentially with increasing distance from the sheet. Consequently, the Coulomb coupling between plasmons on different layers vanishes, if the interlayer distance d in the multilayer is much larger than λ. Hence, the dielectric response of any graphene multilayer resembles that of isolated graphene for large $\bar{q} \gg 2\pi/d$. The range of intermediate momentum transfers $\bar{q}$ is most interesting, as the Coulomb coupling becomes crucial. To understand the characteristic changes of the π-plasmon dispersion with increasing numbers of layers, we extend our previous discussion using a simple dielectric model.

B. Layered-electron-gas model

The layered-electron-gas (LEG) model has been used extensively to study plasmons in layered systems. In the following, we briefly review the theory (see Refs. [7–9,11,18,19]) and adapt the model for momentum-resolved EELS. Within the LEG model, the graphene multilayer is approximated as a stack of N equidistant sheets, which consist of a homogeneous, two-dimensional electron gas and are only coupled via Coulomb interactions. The dielectric function of this model system can be expressed as a $N \times N$ matrix, relating external and total potential on the nth and mth layers by $\phi_n^e = \sum_m \varepsilon_{nm}\phi_m^t$. Starting from the polarizability $\Pi(\bar{\boldsymbol{q}},\omega)$ of a single layer, which depends on the in-plane momentum $\bar{\boldsymbol{q}}$ and energy ω, the elements of the dielectric matrix for a N-layer stack are given by (see Supplemental Material [38])

$$\varepsilon_{nm}(\bar{\boldsymbol{q}},\omega) = \delta_{nm} - v_{2\text{D}}(\bar{q})\, V_{nm}(\bar{q})\, \Pi(\bar{\boldsymbol{q}},\omega), \qquad (1)$$

where $v_{2\text{D}} = 2\pi e^2/\bar{q}$ is the 2D Coulomb potential in a single layer and $V_{nm} = e^{-\bar{q}d|n-m|}$ describes the interaction strength between different sheets. As this coupling matrix $V(\bar{q})$ is real and symmetric, there exists an orthonormal set of eigenvectors $u_n^{(l)}(\bar{q})$ with real eigenvalues $\nu^{(l)}(\bar{q})$. The eigenvectors correspond to the normal modes of the multilayer system and specify the variation of amplitude and phase of the associated potentials across different layers n. They also diagonalize the dielectric matrix ε and the corresponding eigenvalues $\varepsilon^{(l)} = 1 - v_{2\text{D}}\nu^{(l)}\Pi$ can be interpreted as dielectric band structure [42]. Plasmons are supported by the multilayer system if one of these N eigenvalues vanishes, i. e., $\text{Re}\,\varepsilon^{(l)}(\bar{\boldsymbol{q}},\omega^{(l)}) = 0$. For each momentum $\bar{\boldsymbol{q}}$, we may thus find N different plasmon energies $\omega^{(l)}(\bar{\boldsymbol{q}})$ related to the N normal modes $u_n^{(l)}(\bar{q})$ of the stack—these are the so-called *plasmon*

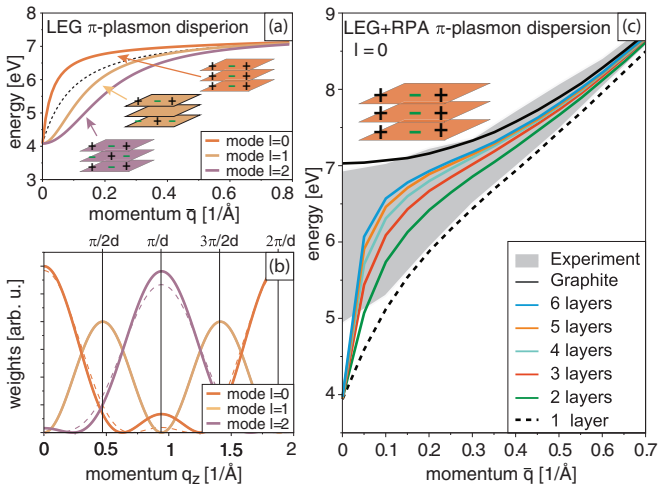

FIG. 2. (Color online) Layered-electron-gas model for the π plasmon in multilayer graphene. (a) For three layers, the plasmon dispersion splits into three plasmon bands. (b) The contribution of a specific band to the energy-loss function in AR-EELS is determined by the weights $|\tilde{u}^{(l)}(\bar{q},q_z)|^2$. The q_z dependence is shown for an in-plane momentum $\bar{q}$ of 0.1 Å^{-1} (solid) and 1 Å^{-1} (dashed lines). (c) Dispersion of the highest-energy plasmon band ($l = 0$) in multilayer graphene with two to six layers calculated using the RPA polarizability of graphene. Experimental results of Fig. 1(b) are indicated in gray.

bands. For illustration, we consider the plasmon bands of three-layer graphene using a simple two-oscillator Lorentz model [18] for the polarizability Π of graphene. As shown in Fig. 2(a), the π-plasmon dispersion of isolated graphene (dashed line) splits into three plasmon bands in the multilayer system (solid lines) which are associated with different charge-oscillation patterns (normal modes) as illustrated by the insets.

Starting from this simple LEG model, we can determine the response of the multilayer to a probing electron beam. In momentum-resolved EELS, the scattered external electron acts as a plane-wave perturbation with momentum transfer $\boldsymbol{q} = \bar{\boldsymbol{q}} + q_z \boldsymbol{e}_z$ and energy ω. Introducing the Fourier coefficients of the eigenvectors $\tilde{u}^{(l)}(\bar{q},q_z) \equiv \sum_n u_n^{(l)}(\bar{q})\, e^{-iq_z nd}$, we obtain for the energy-loss probability (see Supplemental Material [38])

$$P(\bar{\boldsymbol{q}},q_z,\omega) \propto -\frac{1}{q^4}\sum_{l=1}^{N} |\tilde{u}^{(l)}(\bar{q},q_z)|^2 \,\mathrm{Im}\,\frac{\Pi(\bar{\boldsymbol{q}},\omega)}{\varepsilon^{(l)}(\bar{\boldsymbol{q}},\omega)}. \qquad (2)$$

This quantity can be directly compared to a measured energy-loss spectrum at momentum transfer $\boldsymbol{q}$. It is easily understood as a weighted sum of normal-mode spectra $-\mathrm{Im}\,\Pi/\varepsilon^{(l)}$, which are associated with the excitation of a plasmon mode l in the multilayer. The weights $|\tilde{u}^{(l)}(\bar{q},q_z)|^2$ are mainly determined by the out-of-plane momentum transfer q_z and are shown for a three-layer system in Fig. 2(b). For $q_z = 0$, the symmetric plasmon mode $l = 0$ is dominant, because a plane-wave perturbation parallel to the sheets can only excite charge oscillations with the same phase on different planes. Consequently, our experimental results shown in Fig. 1(b) correspond to the plasmon bands with highest energy in each multilayer. However, we find quite important differences to our experimental results. For example, the linear dispersion of the π plasmon in single-layer graphene [29,33] is not correctly reproduced [dotted line in Fig. 2(a)]. This can be traced back to the poor approximation of the polarizability Π using a simple Lorentz model. To improve our results of the LEG model, we instead performed density-functional-theory calculations (see Supplemental Material [38] for details) to obtain quantitative, parameter-free predictions for the polarizability $\Pi(\bar{\boldsymbol{q}},\omega)$ of graphene within the random-phase approximation (RPA). As we have shown earlier [34], these calculations accurately reproduce EELS experiments on freestanding single-layer graphene for finite $\bar{q} > 0.1$ Å^{-1}. Starting from the RPA polarizability of graphene, we calculate energy-loss spectra of multilayer graphene for increasing numbers of layers using Eqs. (1) and (2).

C. Transition between 2D and 3D behavior

Figure 2(c) shows the resulting π-plasmon dispersion in multilayer graphene for in-plane momentum transfers $\bar{\boldsymbol{q}}$ along the ΓM direction. We find very good agreement with our experimental results in Fig. 1(b), which validates the use of the LEG + RPA model to study the thickness dependence of the plasmon dispersion. First, we consider large in-plane momentum transfers $\bar{q} \gg 1/d$. In this case, the coupling $e^{-\bar{q}d}$ between adjacent sheets vanishes and each of the layers supports independent plasmon modes of isolated graphene. One can derive this result from Eq. (1), as V becomes a unit matrix and all eigenvalues approach the dielectric function of isolated graphene, $\varepsilon^{(l)} = 1 - v_{2D}\Pi$. Consequently, in all graphene multilayers, the dispersion curves of all modes converge towards the graphene dispersion for large $\bar{q}$ in accordance with our intuitive picture discussed earlier. This changes for intermediate momentum transfers $\bar{q} \approx 1/d$, where the plasmon modes split in energy due to the interlayer coupling. The splitting increases with the number of layers N. In particular, the highest eigenvalue $v^{(0)}$ of the coupling matrix V can be shown to grow monotonously with N, which in turn raises the corresponding plasmon energy $\omega^{(0)}$ until a limiting value is reached for $N \to \infty$. This explains the thickness dependence of the π and $\pi + \sigma$ plasmon energy for the symmetric $l = 0$ mode, which is probed in our EELS measurements. Note, that for small $\bar{q} \approx 0.1$ Å^{-1} the π-plasmon energy of six-layer graphene still deviates by about 1 eV from the value in graphite. Finally, we consider the optical limit $\bar{q} \to 0$, which shows a very particular behavior: As the polarizability $\Pi \propto \bar{q}^2$ vanishes, the dielectric matrix in Eq. (1) converges towards a unit matrix. Thus, the system cannot support a plasmon mode as $\varepsilon^{(l)}(\omega) \to 1$ never vanishes. Instead, the energy-loss probability in Eq. (2) becomes proportional to the absorption spectrum of graphene $-\mathrm{Im}\,\Pi(\omega)$. This holds for all finite graphene stacks, including single-layer graphene. Experimentally, we do not observe this kind of degeneracy, but find a gradual shift of the π and $\pi + \sigma$ peak to higher energy loss, slowly approaching the position in graphite. This difference indicates a breakdown of the LEG model for $\bar{q} \to 0$, where any multilayer behaves like a 2D system. Alternatively, it can be explained by experimental restrictions that prevent a direct measurement of the actual limit $\bar{q} = 0$ [34].

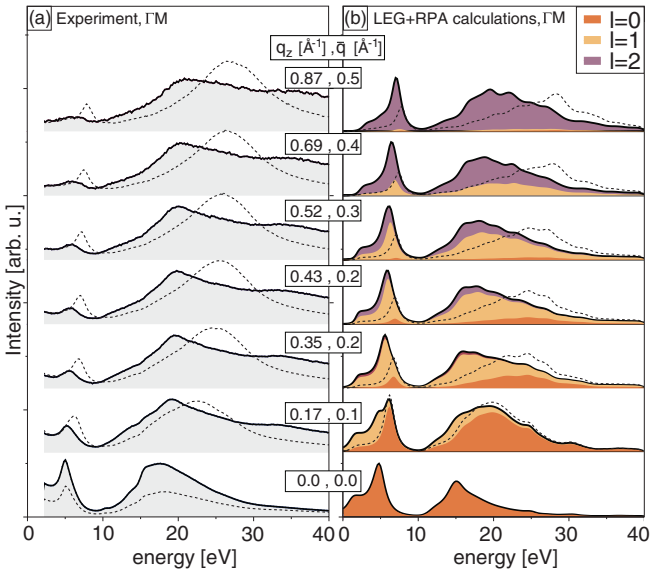

FIG. 3. (Color online) Momentum-resolved energy-loss spectra of tilted (60°) and untilted (0°) three-layer graphene. (a) Comparison of experimental energy-loss spectra for the tilted (solid lines) and untilted (dashed lines) cases with same in-plane momentum $\bar{q}$. (b) Corresponding calculations using the LEG + RPA model. For the tilted case, individual contributions from the three plasmon modes ($l = 0,1,2$) are indicated as colored areas. Untilted spectra correspond to the $l = 0$ mode.

D. Measuring plasmon bands in three-layer graphene

So far, we have only discussed the high-energy mode ($l = 0$) of multilayer graphene. In order to also study the lower-energy modes ($l > 0$), finite out-of-plane momentum transfers $|q_z| > 0.1\,\text{Å}^{-1}$ are required [see Fig. 2(b)]. Experimentally, this can be realized by tilting the sample normal by an angle γ with respect to the electron beam. In this geometry, the total momentum transfer $\boldsymbol{q}$ has both a strong out-of-plane component $q_z = q\,\sin\gamma$ and in-plane component $\bar{q} = q\,\cos\gamma$. To predict the effect of a sample tilt on the measured energy-loss spectra, we have repeated our RPA + LEG calculations for a three-layer graphene system tilted by an angle γ of 60°. Figure 3(b) shows resulting energy-loss spectra (solid lines) for increasing total momentum transfer q, i.e., for increasing $\bar{q}$ and q_z components. We can make three main observations: (i) the π plasmon has a rather small dispersion and is clearly split into two peaks around $q_z \approx 0.2\,\text{Å}^{-1}$, (ii) for $q_z > 0.3\,\text{Å}^{-1}$, the $\pi + \sigma$ plasmon hardly undergoes any further changes in regard to its line shape and energy position, and (iii) compared to the pure in-plane response (dashed lines), i.e., spectra with the same $\bar{q}$ but vanishing q_z, both plasmon peaks are noticeably redshifted. An explanation for these observations can be found by analyzing the partial contributions of all three plasmon modes $l = 0,1,2$ [colored areas in Fig. 3(b)] to the total loss probability. For small q_z, only the $l = 0$ mode is excited, hence the similarity between the tilted and untilted spectra. But with increasing q_z first the $l = 1$ mode becomes stronger, and eventually the $l = 2$ mode dominates the loss probability at large q_z. The reduced dispersion of the π plasmon and the almost unchanged $\pi + \sigma$ plasmon in the tilted case, can thus be traced back to two competing effects: All plasmon modes gradually shift to higher energies with increasing $\bar{q}$, but with increasing q_z low-energy modes ($l > 0$) start to dominate the loss probability, shifting the plasmon peaks back to lower energies compared to the pure in-plane spectrum ($l = 0$). Most interestingly, we find certain momentum transfers q_z, where only a single mode dominates the loss probability, i.e., $l = 0$ at $q_z \to 0$, $l = 1$ at $q_z \approx 0.45\,\text{Å}^{-1}$, and $l = 2$ at $q_z \approx 0.9\,\text{Å}^{-1}$. This is also confirmed by the weights $|\tilde{u}^{(l)}|^2$ plotted in Fig. 2(b): Depending on the number of layers N, the weight of a mode l has a maximum around $q_z^{(l)} \approx \frac{\pi}{d}\frac{l}{N-1}$ where it dominates the energy-loss probability. Consequently, the dispersion of all plasmon bands can, in principle, be measured by choosing different sample tilt angles in order to vary $\bar{q}$ while keeping q_z constant.

In order to validate our theoretical predictions, we have performed EELS measurements on tilted three-layer graphene samples [see Fig. 3(a)]. For a direct comparison between the tilted (solid lines) and untilted case (dashed lines), all spectra were normalized to the same electron dose per unit area. Our measurements show the same principal trends as our calculations: (i) a significantly smaller π-plasmon dispersion in the tilted case, (ii) an almost nondispersing and triangular-shaped $\pi + \sigma$ plasmon, and (iii) the same strong redshifts of both plasmons when compared to the pure in-plane response. This good agreement between theory and experiment shows that it is indeed possible to measure individual, lower-energy eigenmodes at $q_z \approx 0.45\,\text{Å}^{-1}$ ($l = 1$) and $q_z \approx 0.9\,\text{Å}^{-1}$ ($l = 2$). Therefore, by repeating this experiment at different tilt angles γ, the energy of each plasmon mode can be determined for different in-plane momentum transfers $\bar{q}$, and as such the dispersion of all individual plasmon bands can be derived.

Finally, we also point out differences between our experimental and theoretical results in the tilted case: First, we do not observe any splitting of the π plasmon in our measured energy-loss spectra. This is most likely related to the finite energy and momentum resolution. Second, our experiments show a much lower π-plasmon intensity compared to the $\pi + \sigma$ peak, a notably higher intensity above 30 eV, and an additional peak at 35 eV. We attribute these differences to the out-of-plane polarization of graphene, which is not included in the layered-electron-gas model. A detailed discussion of this point is beyond the scope of this paper and will be investigated in due course.

IV. CONCLUSIONS

We presented a joint experimental and theoretical investigation of plasmon bands in multilayer graphene. The behavior of the highest-energy plasmon mode was studied for graphene stacks with increasing numbers of layers, ranging from the ideal 2D system to a layered 3D bulk material. To this end, the thickness dependence of the π-plasmon dispersion was measured by momentum-resolved electron energy-loss spectroscopy. Our experimental results could be explained quantitatively by means of a simple layered-electron-gas model, which was combined with *ab initio* calculations for graphene. We showed that the observed thickness dependence is governed by interlayer Coulomb interactions. Further, we found that momentum-resolved energy-loss spectra for

N-layer graphene can be understood as the weighted sum of N eigenspectra, which are directly related to the plasmon bands in the system. For standard scattering geometries (normal incidence), only the highest-energy plasmon band is excited. Plasmon modes with lower energies can only contribute for finite out-of-plane momentum transfers q_z. We identified conditions where the energy-loss probability is dominated by a single plasmon mode and proposed a method to measure all individual plasmon bands by momentum-resolved energy-loss spectroscopy on tilted samples. As a proof of concept, we performed model calculations and experiments for a tilted three-layer graphene system. The good agreement between theory and experiment shows that momentum-resolved EELS is an ideal tool to map plasmon bands in 2D-based heterostructures.

ACKNOWLEDGMENTS

The authors gratefully acknowledge financial support by the German Research Foundation (DFG) and the Ministry of Science, Research and Arts (MWK) of the state Baden-Württemberg within the Sub-Angstrom Low-Voltage Electron Microscopy project (SALVE).

[1] F. Bonaccorso, Z. Sun, T. Hasan, and A. C. Ferrari, Nat. Photonics **4**, 611 (2010).
[2] F. J. García de Abajo, ACS Photon. **1**, 135 (2014).
[3] Z. Fang, Z. Liu, Y. Wang, P. Ajayan, P. Nordlander, and N. Halas, Nano Lett. **12**, 3808 (2012).
[4] Z. Sun, T. Hasan, F. Torrisi, D. Popa, G. Privitera, F. Wang, F. Bonaccorso, D. M. Basko, and A. C. Ferrari, ACS nano **4**, 803 (2010).
[5] K. S. Novoselov, V. I. Fal'ko, L. Colombo, P. R. Gellert, M. G. Schwab, and K. Kim, Nature (London) **490**, 192 (2012).
[6] A. K. Geim and I. V. Grigorieva, Nature (London) **499**, 419 (2013).
[7] A. L. Fetter, Ann. Phys. (NY) **88**, 1 (1974).
[8] S. Das Sarma and J. J. Quinn, Phys. Rev. B **25**, 7603 (1982).
[9] W. L. Bloss and E. M. Brody, Solid State Commun. **43**, 523 (1982).
[10] R. E. Camley and D. L. Mills, Phys. Rev. B **29**, 1695 (1984).
[11] G. F. Giuliani, P. Hawrylak, and J. J. Quinn, Phys. Scr. **36**, 946 (1987).
[12] S.-J. Cheng and R. R. Gerhardts, Phys. Rev. B **63**, 035314 (2001).
[13] D. Olego, A. Pinczuk, A. C. Gossard, and W. Wiegmann, Phys. Rev. B **25**, 7867 (1982).
[14] R. Sooryakumar, A. Pinczuk, A. Gossard, and W. Wiegmann, Phys. Rev. B **31**, 2578 (1985).
[15] G. Fasol, R. D. King-Smith, D. Richards, U. Ekenberg, N. Mestres, and K. Ploog, Phys. Rev. B **39**, 12695 (1989).
[16] T. Neyer, P. Schattschneider, J. P. R. Bolton, and G. A. Botton, J. Micr. **187**, 184 (1997).
[17] T. Neyer, G. A. Botton, D. Su, P. Schattschneider, J. P. R. Bolton, and E. Ziegler, in *IOP Conf. Proc. No. 153* (IOP Publishing LTD, UK, 1997), pp. 363–366.
[18] V. B. Jovanović, I. Radović, D. Borka, and Z. L. Mišković, Phys. Rev. B **84**, 155416 (2011).
[19] J.-J. Zhu, S. M. Badalyan, and F. M. Peeters, Phys. Rev. B **87**, 085401 (2013).
[20] J. Lu, K. P. Loh, H. Huang, W. Chen, and A. T. S. Wee, Phys. Rev. B **80**, 113410 (2009).
[21] Y. Liu and R. F. Willis, Phys. Rev. B **81**, 081406 (2010).
[22] H. Pfnür, T. Langer, J. Baringhaus, and C. Tegenkamp, J. Phys.: Condens. Matter **23**, 112204 (2011).
[23] M. Gass, U. Bangert, A. Bleloch, P. Wang, R. Nair, and A. K. Geim, Nat. Nanotechnol. **3**, 676 (2008).
[24] T. Eberlein, U. Bangert, R. R. Nair, R. Jones, M. Gass, A. L. Bleloch, K. S. Novoselov, A. Geim, and P. R. Briddon, Phys. Rev. B **77**, 233406 (2008).
[25] L. Yang, J. Deslippe, C.-H. Park, M. L. Cohen, and S. G. Louie, Phys. Rev. Lett. **103**, 186802 (2009).
[26] L. Yang, Phys. Rev. B **83**, 085405 (2011).
[27] Z. Chen and X.-Q. Wang, Phys. Rev. B **83**, 081405(R) (2011).
[28] S. Yuan, R. Roldán, and M. I. Katsnelson, Phys. Rev. B **84**, 035439 (2011).
[29] C. Kramberger, R. Hambach, C. Giorgetti, M. H. Rümmeli, M. Knupfer, J. Fink, B. Büchner, L. Reining, E. Einarsson, S. Maruyama, F. Sottile, K. Hannewald, V. Olevano, A. G. Marinopoulos, and T. Pichler, Phys. Rev. Lett. **100**, 196803 (2008).
[30] J. Yan, K. S. Thygesen, and K. W. Jacobsen, Phys. Rev. Lett. **106**, 146803 (2011).
[31] Y. Gao and Z. Yuan, Solid State Commun. **151**, 1009 (2011).
[32] V. Despoja, D. Novko, K. Dekanić, M. Šunjić, and L. Marušić, Phys. Rev. B **87**, 075447 (2013).
[33] M. K. Kinyanjui, C. Kramberger, T. Pichler, J. C. Meyer, P. Wachsmuth, G. Benner, and U. Kaiser, Europhys. Lett. **97**, 57005 (2012).
[34] P. Wachsmuth, R. Hambach, M. K. Kinyanjui, M. Guzzo, G. Benner, and U. Kaiser, Phys. Rev. B **88**, 075433 (2013).
[35] J. Meyer, C. O. Girit, M. F. Crommie, and A. Zettl, Appl. Phys. Lett. **92**, 123110 (2008).
[36] U. Kaiser, J. Biskupek, J. Meyer, J. Leschner, L. Lechner, H. Rose, M. Stöger-Pollach, A. Khlobystov, P. Hartel, H. Müller, M. Haider, S. Eyhusen, and G. Benner, Ultramicroscopy **111**, 1246 (2011).
[37] P. Wachsmuth, Ph.D. thesis, Ulm University, 2014.
[38] See Supplemental Material at http://link.aps.org/supplemental/10.1103/PhysRevB.90.235434 for details on the experimental and numerial methods.
[39] K. Zeppenfeld, Phys. Lett. A **25**, 335 (1967).
[40] A. G. Marinopoulos, L. Reining, A. Rubio, and V. Olevano, Phys. Rev. B **69**, 245419 (2004).
[41] W. Zhou, J. Lee, J. Nanda, S. Pantelides, S. Pennycook, and J.-C. Idrobo, Nat. Nanotechnol. **7**, 161 (2012).
[42] R. Car, E. Tosatti, S. Baroni, and S. Leelaprute, Phys. Rev. B **24**, 985 (1981).